

Photodiodes based in La_{0.7}Sr_{0.3}MnO₃ /single layer MoS₂ hybrid vertical heterostructures

Yue Niu^{1,2}, Riccardo Frisenda¹, Simon A. Svatek^{1,5}, Gloria Orfila^{3,4,7}, Fernando Gallego^{6,7}, Patricia Gant¹, Nicolás Agrait^{1,5}, Carlos León^{3,4,7}, Alberto Rivera-Calzada^{3,4,7}, David Perez De Lara¹, Jacobo Santamaria^{3,4,7,*} Andres Castellanos-Gomez^{6,*}

¹ Instituto Madrileño de Estudios Avanzados en Nanociencia (IMDEA-Nanociencia), Faraday 9, Ciudad Universitaria de Cantoblanco, 28049 Madrid, Spain.

² National Key Laboratory of Science and Technology on Advanced Composites in Special Environments, Harbin Institute of Technology, Harbin, China

³ GFMC, Departamento de Física de Materiales. Universidad Complutense de Madrid, 28040 Madrid, Spain.

⁴ GFMC, Instituto de Magnetismo Aplicado “Salvador Velayos”, Universidad Complutense de Madrid, 28040 Madrid, Spain.

⁵ Departamento de Física de la Materia Condensada and IFIMAC. Universidad Autónoma de Madrid, Madrid, E-28049, Spain.

⁶ Instituto de Ciencia de Materiales de Madrid (ICMM-CSIC), Sor Juana Ines de la Cruz, 3, Cantoblanco, 28049 Madrid, Spain.

⁷ Unidad Asociada “Laboratorio de heteroestructuras con aplicacion en espintronica”, UCM/CSIC, Sor Juana Ines de la Cruz, 3, Cantoblanco, 28049 Madrid, Spain

E-mail: Jacobo Santamaría: jacsan@fis.ucm.es . Andres Castellanos-Gomez : andres.castellanos@csic.es

ABSTRACT

The fabrication of artificial materials by stacking of individual two-dimensional (2D) materials is amongst one of the most promising research avenues in the field of 2D materials. Moreover, this strategy to fabricate new man-made materials can be further extended by fabricating hybrid stacks between 2D materials and other functional materials with different dimensionality making the potential number of combinations almost infinite. Among all these possible combinations, mixing 2D materials with transition metal oxides can result especially useful because of the large amount of interesting physical phenomena displayed separately by these two material families. We present a hybrid device based on the stacking of a single layer MoS₂ onto a lanthanum strontium manganite (La_{0.7}Sr_{0.3}MnO₃) thin film, creating an atomically thin device. It shows a rectifying electrical transport with a ratio of 10³, and a photovoltaic effect with V_{oc} up to 0.4 V. The photodiode behaviour arises as a consequence of the different doping character of these two materials. This result paves the way towards combining the efforts of these two large materials science communities.

Since the first experimental isolation of graphene in 2014¹, the interest on other layered 2D materials has kept growing²⁻⁴. Moreover, the community working on 2D materials is rapidly moving from the fundamental study of these atomically thin materials towards integrating them with other advanced materials to create hybrid devices. The case where an artificial layered material is created by stacking two different individual 2D layers results highly appealing⁵⁻¹⁰, but also a great deal of experimental efforts have been paid to fabricate hybrid devices by combining 2D materials with other functional materials¹¹. Lopez-Sanchez et al. and Gehring et al., for instance, fabricated artificial heterostructures by stacking 2D semiconductors on top of conventional 3D semiconductors¹²⁻¹⁴, Velez et al. combined MoS₂ with organic semiconductors¹⁵ and Jariwala et al. fabricated hybrid devices by combining mechanically exfoliated MoS₂ flakes with a carbon nanotube film¹⁶.

Transition Metal Oxides (TMO), sometimes called simply complex oxides, constitute a very interesting family of materials because they display very different physical phenomena like superconductivity, ferroelectricity, ferro and antiferromagnetism, etc. The strong correlation between the several degrees of freedom of TMO (charge, spin, strain, doping) produces a rich variety of phases which result in complex phase diagrams^{17,18}. Manganites are one of the paradigmatic examples of TMO showing a characteristic magnetoresistance behavior. Therefore, the combination of 2D materials with TMO is very prospective because of the rich physical phenomena that both families present separately, but the amounts of works on 2D materials/TMO heterostructures are still very scarce.

In this work we fabricate a vertical heterostructure by transferring a single-layer MoS₂ flake on top of a La_{0.7}Sr_{0.3}MnO₃ (LSMO) thin film, epitaxially grown on a SrTiO₃ (STO) substrate. We study the electrical transport properties of the heterostructure that behaves as a diode because of the junction between the LSMO film and MoS₂. This junction presents an electrical rectifying behavior (with a rectification ratio, R.R., of $\sim 10^3$) and upon illumination it shows photovoltaic effect. These results constitute the first steps towards combining these two large families of functional materials, opening the door for many possible 2D materials/complex oxide hybrid devices.

The LSMO film was grown by high pressure pure oxygen (3.2 mbar) RF sputtering at 900 °C on (001) oriented optically polished SrTiO₃ substrates. The LSMO layer was fully epitaxial and uniformly strained and had a ferromagnetic ground state. Details about sample properties and growth can be found elsewhere¹⁹. For the device fabrication, the LSMO film was patterned by electron beam lithography to form mesas. Firstly, MaN-2403 negative resist was spin coated on the sample, and the pattern was exposed to the electron beam. After the development of the resist, the material was etched

resulting in the bottom LSMO nanostructured layer. The bottom (LSMO) electrical contact was defined evaporating Ag through a mechanical mask. Silver electrodes were checked to provide ohmic contacts to the LSMO film in agreement with previous results²⁰.

The structural quality of the sample was analyzed by X-ray diffraction (XRD) obtaining the pattern shown in the top inset to Figure 1. A zoom to the 001 reflection of the STO substrate is presented, showing the 001 peak of the film, and many lateral fringes at both sides, indicating the high crystalline quality of the LSMO film. In the main panel of Figure 1, the X-ray reflectivity (XRR) of the LSMO layer is plotted, presenting again many oscillations up to over 5 degrees in 2θ , as a consequence of the flatness of the film. The spacing of the maxima is a function of the thickness of the film, yielding a value of 28 ± 1 nm. The lower inset in Figure 1 presents the 3D AFM image of the etched LSMO mesa on which the MoS₂ will be deposited, showing the sharp edges of the LSMO nanostructure and confirming the thickness of the layer (28 ± 1 nm).

The single layer MoS₂ flake was deposited onto a polydimethylsiloxane (PDMS) stamp (Gelfilm by Gelpak) by mechanical exfoliation of a bulk molybdenite natural crystal (Holly Mill mine, Canada) with a SPV 224 Nitto tape. The single layer region is identified at glance by its optical contrast in transmission mode microscopy and the number of layers is double checked by quantitative analysis of the transmission mode images and by determining the energy of the A, B and C excitons from micro-reflectance spectroscopy^{21,22}. Figure 2(a) shows a transmission mode optical image of the MoS₂ flake onto the PDMS stamp prior to transfer (the inset shows the transmission mode image of the same flake transferred onto the LSMO film). Figure 2(b) shows the micro-reflectance spectra acquired on the MoS₂ flake before being transferred to the LSMO surface, used to determine the number of MoS₂ layers. Then the flake was transferred onto the LSMO surface by an all-dry deterministic transfer technique, described in detail in Ref.²³.

The electrical transport properties of the MoS₂/LSMO stack are characterized with a homebuilt probe station equipped with carbon fiber microprobes that can be accurately placed onto mechanically exfoliated flakes (the diameter of the fiber microprobes is of only 7 μ m) without damaging them. Their Young modulus is ~ 280 GPa and the spring constant of a typical carbon fiber probe (~ 1 mm long) is ~ 0.02 N/m,^{24,25} allowing for very gentle mechanical contact without damaging the flakes. The electrical contact between a carbon fiber probe and MoS₂ flakes has been reported to be Ohmic²⁶. More details on this experimental setup and measurements can be found in Ref.²⁶. Figure 2(c) is a sketch of the experimental configuration employed to probe the electrical properties of the stack. A source measure unit (Keithley 2450) is used to perform the current-voltage measurements. The light source is provided by a high-power LED source (455 nm of

illumination wavelength with a power density up to 0.64 W/cm²).

Figure 3 shows the current vs. bias voltage trace (*IV* hereafter) measured in the dark state, showing a marked rectifying behavior. The inset in Figure 3 displays the same *IV* in logarithmic scale (with the current in absolute value) to facilitate the estimation of the rectification ratio of the diode. The device, despite of being atomically thin, presents a very large rectification ratio of $\sim 10^3$. Note that Ag and LSMO have very similar work functions (4.7 eV and 4.8 eV respectively), and thus Ag acts as a good ohmic contact to LSMO¹⁹. On the contrary, the electron affinity of MoS₂ is lower (4.2 eV). Moreover, the Fermi level in LSMO is close to valence band and in MoS₂ the Fermi level is quite close to the conduction band. Therefore, the LSMO behavior can be described as a hole metal (P⁺⁺), and the MoS₂ a N⁺ semiconductor. It is therefore expected that electrons are transferred in the junction from the MoS₂ into the LSMO, eventually leading to a decrease in the concentration of electrons in MoS₂. Similar charge transfer has been observed in other metal oxide - transition metal dichalcogenide interfaces^{27,28}. Nevertheless, our results indicate that in the MoS₂/LSMO junctions the MoS₂ behaves as the N side and LSMO as the P side of a diode. In general, in atomically thin PN-junctions there is no built-in field and thus the carrier transport occurs by tunneling processes⁵. However, in this case the thickness of the LSMO film allows carrier diffusion and drift processes. Therefore, a built-in field may be generated in the LSMO side to level the chemical potentials. Notice the reversibility of *IV* curves measured sequentially in the dark (Supporting Information, Figure S6 and S7) excludes oxygen vacancy generation in the range of applied electric fields of the experiment, which would show up in the *IV* curves as resistive switching effects²⁹. Assuming that the voltage corresponding to the difference between the work functions of both materials drops in a space charge region in the LSMO of a width of the Thomas Fermi screening length (typically between 1 and 2 nm), an electric field can be estimated in the range $2\text{-}5 \times 10^6 \text{ V}\cdot\text{cm}^{-1}$. This field is screened by a sheet carrier density of the order 10^{12} cm^{-2} quite close to the typical values of the sheet carrier density of MoS₂³⁰.

After characterizing diode-like electrical transport properties of the stacked device we study the performance of the device upon illumination. We project a high-power LED source, forming a spot of 400 μm in diameter, onto the stacked MoS₂/LSMO. Figure 4(a) shows the *IV* characteristics of the device in dark and upon illumination with increasingly high power density. The forward current increases monotonically with the illumination power density because of the photogeneration of electron-hole pairs that are separated by the applied drain-source bias voltage (photoconductive generation mechanism). At zero applied bias, the built-in electric field in the interface (due to the different doping character of the two materials) separates the photogenerated electron-hole pairs producing a finite current (so called I_{sc} short circuit current), which is a fingerprint of the photovoltaic effect. We ruled out the photogeneration of current at the Ag/LSMO and

carbon fibre/MoS₂ interfaces as they present Ohmic contact behavior.^{19,26} Although scanning photocurrent mapping could be an independent way to proof the negligible effect of the Ag/LSMO and carbon fibre/MoS₂ interfaces in the photocurrent generation but its implementation in combination with the carbon fiber top electrode results technically challenging and it lays beyond the scope of this manuscript. The voltage (at zero current) generated in the junction upon illumination (open circuit voltage, V_{oc}) and it is another characteristic of the photovoltaic effect. Figure 4(b) shows a zoom in the I/V characteristics of Figure 4(a) to facilitate the identification of the short circuit current and open circuit voltage generated upon illumination. Figure 4(c) shows the optical power dependence of these values displaying a linear dependence for I_{sc} and logarithmic dependence for V_{oc} , characteristics of photodiodes. The V_{oc} saturates at values close to 0.4 V even without optimizing the carrier extraction electrodes. The comparison with other heterojunctions in the literature shows that the V_{oc} value of our complex oxide/2D semiconductor is comparable to that of other devices based on vertical stacking of 2D semiconductors (see Table 1) and also the filling factor (FF) of our device is the largest reported so far for these kind of vertical heterostructure devices. Table 1 also compares the short circuit current density of different devices. Note that in our device the contact area is not well-defined but considering an area of 50 μm^2 (a conservative value taking into account the diameter of 7 μm of the fiber) the J_{sc} value of our device is $\sim 1 \text{ mA/cm}^2$, which is a moderate value compared with other vertical heterostructure. Nonetheless, our device also presents a unique feature: the whole stack is almost transparent (see inset in Figure 2(a)) while the rest of listed stacks are fabricated on top of opaque substrates.

In summary, we presented a hybrid device based on the artificial stacking of single-layer MoS₂ onto a LSMO thin film. The different doping character of these materials is exploited to build up an atomically thin photodiode device that shows a remarkably high rectification ratio ($\sim 10^3$) and upon illumination displays photovoltaic effect with V_{oc} up to 0.4 V. The results presented here constitute the first step towards combining the efforts of two large materials science communities, the two-dimensional materials and the TMO to fabricate optimized artificial materials combining suitable members of each family.

Acknowledgements

Work at IMDEA was supported by MINECO (Ramón y Cajal 2014 program RYC-2014-01406, MAT2014-58399-JIN, FIS2015-67367-C2-1-P), the Comunidad de Madrid (MAD2D-CM Program (S2013/MIT-3007)) and NANOFRONTMAG-CM program (S2013/MIT-2850) and the European Commission under the Graphene Flagship (contract CNECTICT-604391) and FP7 ITN MOLESCO (project no. 606728). RF acknowledges support from the

Netherlands Organisation for Scientific Research (NWO) through the research program Rubicon with project number 680-50-1515. YN acknowledges the grant from the China Scholarship Council (File NO. 201506120102). Work at UCM supported by Spanish MINECO through grants MAT2014-52405-C02-01 and by CAM through grant CAM S2013/MIT-2740. Work at ICMM is supported by Spanish MINECO through grant MAT2014-52405-C02-02

Supporting Information:

Supporting Information includes:

- 1) Thickness determination from differential reflectance data and quantitative analysis of the transmission mode images
- 2) Determination of the resistance of the carbon fiber probe
- 3) Electrical power generated through the photovoltaic effect
- 4) Measurements on another MoS₂/LSMO device
- 5) Measurements on multilayer MoS₂/LSMO devices
- 6) Current vs. voltage characteristics of a LSMO device with silver contacts

Figures

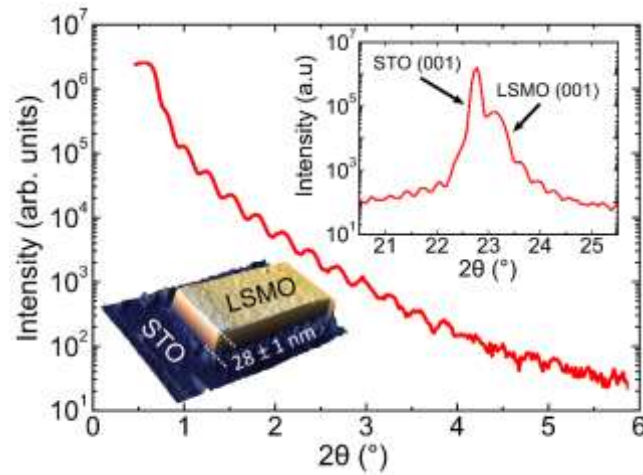


Figure 1 X-ray diffraction pattern (top inset), and reflectivity (main) of a 28 nm LSMO film grown on STO (001) substrate. The bottom inset is an AFM 3D image of the mesa that will contain the MoS₂ flake.

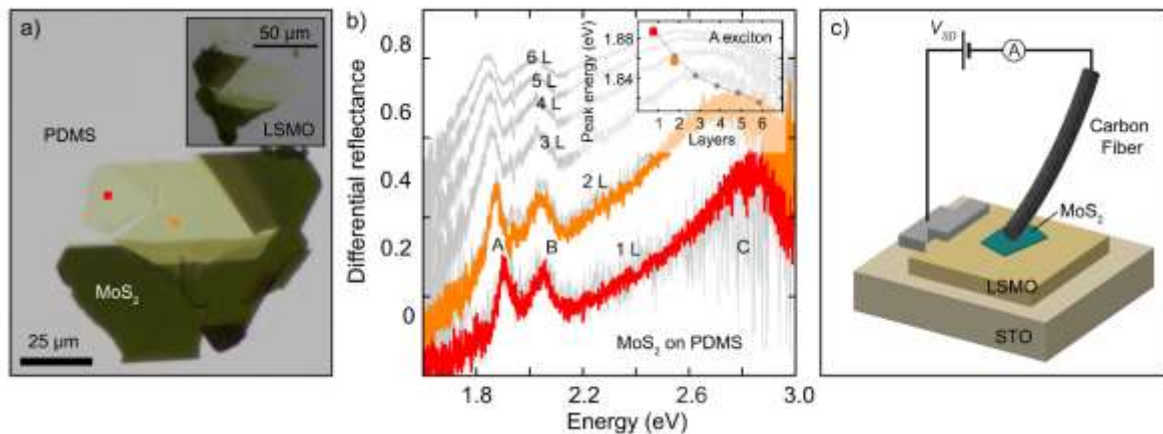


Figure 2 (a) Transmission mode optical image of a MoS₂ flake on a PDMS stamp before its transfer and after being transferred onto the LSMO thin film (inset). (b) Differential reflectance spectra measured on the MoS₂ flake before its transfer to determine its number of layers. The spectra in red and orange have been acquired at the positions highlighted with squares of the same color in (a). The panel also includes the spectra acquired for reference MoS₂ samples with different number of layers (gray). The inset in (b) shows the comparison between the energy of the A exciton measured at the locations shown in (a) and on the reference samples to determine the number of layers. (c) Sketch of the experimental configuration to measure the electrical transport across the MoS₂/LSMO stack.

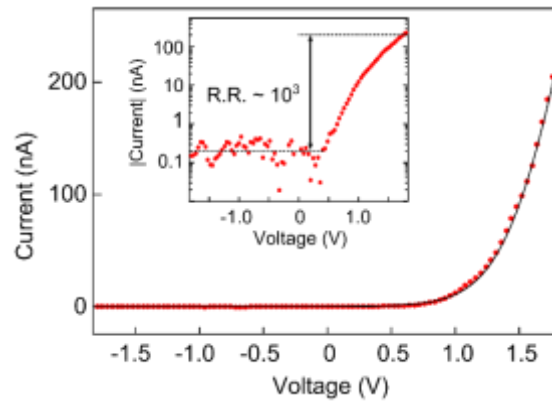


Figure 3 Current vs. bias voltage characteristics of the single-layer MoS₂/LSMO device. The inset shows the same dataset in semi-logarithmic scale and displaying the absolute value of the current.

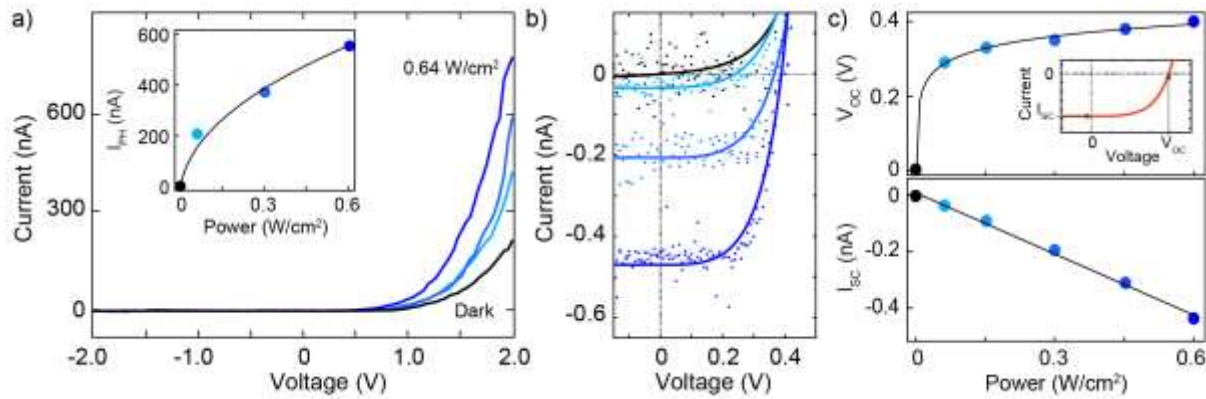


Figure 4 (a) Current vs. bias voltage characteristics of the device in dark and upon illumination with increasingly high illumination power density. The inset shows the photogenerated current vs. the power density. (b) A zoomed in plot around zero bias to show the photovoltaic effect upon illumination. (c) Power dependence of the open circuit voltage and the short circuit current. Illumination wavelength 455 nm.

Vertical stack		V_{oc} (Volts)	J_{sc} (mA/cm ²)	F.F.(%)	Reference
2D/3D semiconductor	1L-MoS ₂ /p-Si	0.41	22.4	0.57	31
	1L-MoS ₂ /p-Si	0.55	100	0.1	13
	FL-BP/GaAs	0.55	10000	0.30	14
	FL-Bi ₂ Te ₃ /p-Si	0.24	0.96	0.38	32
2D/complex oxide	1L-MoS ₂ /28 nm LSMO	0.40	1.0	0.69	This work
2D/organic semiconductor	2L-MoS ₂ /Cu-phthalocyanine	0.60	0.25	0.26	15
2D/2D	1L-MoS ₂ /1L WSe ₂	0.45	0.85	0.29	5
	1L-MoS ₂ /1L WSe ₂	0.55	0.52	0.49	33
	FL-MoS ₂ /FL-WSe ₂	0.27	1000	0.44	34
	1L-MoS ₂ /FL-BP	0.30	9.5	0.32	8

Table 1. Comparison between the open circuit voltages reported for vertical PN junction devices based on the stacking of semiconducting 2D materials.

References

1. Novoselov, K. S. *et al.* Electric field effect in atomically thin carbon films. *Science* **306**, 666–669 (2004).
2. Castellanos-Gomez, A. Why all the fuss about 2D semiconductors? *Nat. Photonics* **10**, 202–204 (2016).
3. Wang, Q. H., Kalantar-Zadeh, K., Kis, A., Coleman, J. N. & Strano, M. S. Electronics and optoelectronics of two-dimensional transition metal dichalcogenides. *Nat. Nanotechnol.* **7**, 699–712 (2012).
4. Lv, R. *et al.* Transition Metal Dichalcogenides and Beyond: Synthesis, Properties, and Applications of Single- and Few-Layer Nanosheets. *Acc. Chem. Res.* **48**, 56–64 (2015).
5. Lee, C.-H. *et al.* Atomically thin p–n junctions with van der Waals heterointerfaces. *Nat. Nanotechnol.* **9**, 676–681 (2014).
6. Withers, F. *et al.* Light-emitting diodes by band-structure engineering in van der Waals heterostructures. *Nat. Mater.* **14**, 301–306 (2015).
7. Massicotte, M. *et al.* Picosecond photoresponse in van der Waals heterostructures. *Nat. Nanotechnol.* **11**, 42–46 (2016).
8. Deng, Y. *et al.* Black Phosphorus-Monolayer MoS₂ van der Waals Heterojunction P-N Diode. *ACS Nano* **8**, 8292–8299 (2014).
9. Yan, R. *et al.* Esaki Diodes in van der Waals Heterojunctions with Broken-Gap Energy Band Alignment. *Nano Lett.* **15**, 5791–8 (2015).
10. Cui, X. *et al.* Multi-terminal transport measurements of MoS₂ using a van der Waals heterostructure device platform. *Nat. Nanotechnol.* **10**, 534–540 (2015).
11. Jariwala, D., Marks, T. J. & C., H. M. Mixed-dimensional van der Waals heterostructures. *Nat. Mater.* (2016).
12. Lopez-Sanchez, O., Dumcenco, D., Charbon, E. & Kis, A. Avalanche photodiodes based on MoS₂/Si heterojunctions. (2014).
13. Lopez-Sanchez, O. *et al.* Light Generation and Harvesting in a van der Waals Heterostructure. *ACS Nano* **8**, 3042–3048 (2014).
14. Gehring, P., Urcuyo, R., Duong, D. L., Burghard, M. & Kern, K. Thin-layer black phosphorous/GaAs heterojunction p-n diodes. *Appl. Phys. Lett.* **106**, 233110 (2015).
15. Vélez, S. *et al.* Gate-tunable diode and photovoltaic effect in an organic-2D layered material p-n junction. *Nanoscale* **7**, 15442–9 (2015).
16. Jariwala, D. *et al.* Gate-tunable carbon nanotube-MoS₂ heterojunction p-n diode. *Proc. Natl. Acad. Sci. U. S. A.* **110**, 18076–80 (2013).
17. Dagotto, E. Complexity in Strongly Correlated Electronic Systems. *Science* **309**, (2005).
18. Tokura, Y. Critical features of colossal magnetoresistive manganites. *Reports Prog. Phys.* **69**, 797–851 (2006).

19. Bruno, F. Y. *et al.* Electronic and Magnetic Reconstructions in La_{0.7} Sr_{0.3} MnO₃ / SrTiO₃ Heterostructures: A Case of Enhanced Interlayer Coupling Controlled by the Interface. *Phys. Rev. Lett.* **106**, 147205 (2011).
20. Bruno, F. Y. *et al.* Effects of interface states on the transport properties of all-oxide La_{0.8}Sr_{0.2}CoO₃/SrTi_{0.99}Nb_{0.01}O₃ p-n heterojunctions. *Appl. Phys. Lett.* **92**, 82106 (2008).
21. Frisenda, R. *et al.* Micro-reflectance and transmittance spectroscopy: a versatile and powerful tool to characterize 2D materials. *J. Phys. D: Appl. Phys.* **50**, 74002 (2017).
22. Ghasemi, F. *et al.* High Throughput Characterization of Epitaxially Grown Single-Layer MoS₂. *Electronics* **6**, 28 (2017).
23. Castellanos-Gomez, A. *et al.* Deterministic transfer of two-dimensional materials by all-dry viscoelastic stamping. *2D Mater.* **1**, 11002 (2014).
24. Castellanos-Gomez, A., Agrait, N. & Rubio-Bollinger, G. Carbon fibre tips for scanning probe microscopy based on quartz tuning fork force sensors. *Nanotechnology* **21**, 145702 (2010).
25. Castellanos-Gomez, A. A simple method to characterize the electrical and mechanical properties of micro-fibers. *Eur. J. Phys.* **34**, 1547–1554 (2013).
26. Gant, P. *et al.* Lithography-free electrical transport measurements on 2D materials by direct microprobing. *J. Mater. Chem. C* (2017). doi:10.1039/C7TC01203A
27. Kaushik, N., Karmakar, D., Nipane, A., Karande, S. & Lodha, S. Interfacial n-Doping Using an Ultrathin TiO₂ Layer for Contact Resistance Reduction in MoS₂. *ACS Appl. Mater. Interfaces* **8**, 256–263 (2016).
28. Zhou, C. *et al.* Carrier Type Control of WSe₂ Field-Effect Transistors by Thickness Modulation and MoO₃ Layer Doping. *Adv. Funct. Mater.* **26**, 4223–4230 (2016).
29. Waser, R. & Aono, M. Nanoionics-based resistive switching memories. *Nat. Mater.* **6**, 833–840 (2007).
30. Castellanos-Gomez, A. *et al.* Electric-field screening in atomically thin layers of MoS₂: The role of interlayer coupling. *Adv. Mater.* **25**, 899–903 (2013).
31. Tsai, M. L. *et al.* Monolayer MoS₂ heterojunction solar cells. *ACS Nano* **8**, 8317–8322 (2014).
32. Wang, Z., Li, M., Yang, L., Zhang, Z. & Gao, X. P. A. Broadband photovoltaic effect of n-type topological insulator Bi₂Te₃ films on p-type Si substrates. *Nano Res.* 1–8 (2016). doi:10.1007/s12274-016-1369-2
33. Furchi, M. M., Pospischil, A., Libisch, F., Burgdörfer, J. & Mueller, T. Photovoltaic Effect in an Electrically Tunable van der Waals Heterojunction. *Nano Lett.* **14**, 4785–4791 (2014).
34. Cheng, R. *et al.* Electroluminescence and photocurrent generation from atomically sharp WSe₂/MoS₂ heterojunction p-n diodes. *Nano Lett.* **14**, 5590–7 (2014).

Supporting Information:

Photodiodes based in La_{0.7}Sr_{0.3}MnO₃ /single layer MoS₂ hybrid vertical heterostructures

Yue Niu^{1,2}, Riccardo Frisenda¹, Simon A. Svatek^{1,5}, Gloria Orfila^{3,4,7}, Fernando Gallego^{6,7}, Patricia Gant¹, Nicolás Agrait^{1,5}, Carlos León^{3,4,7}, Alberto Rivera-Calzada^{3,4,7}, David Perez De Lara¹, Jacobo Santamaria^{3,4,7,*} Andres Castellanos-Gomez^{6,*}

¹ Instituto Madrileño de Estudios Avanzados en Nanociencia (IMDEA-Nanociencia), Faraday 9, Ciudad Universitaria de Cantoblanco, 28049 Madrid, Spain.

² National Key Laboratory of Science and Technology on Advanced Composites in Special Environments, Harbin Institute of Technology, Harbin, China

³ GFMC, Departamento de Física de Materiales. Universidad Complutense de Madrid, 28040 Madrid, Spain.

⁴ GFMC, Instituto de Magnetismo Aplicado “Salvador Velayos”, Universidad Complutense de Madrid, 28040 Madrid, Spain.

⁵ Departamento de Física de la Materia Condensada and IFIMAC. Universidad Autónoma de Madrid, Madrid, E-28049, Spain.

⁶ Instituto de Ciencia de Materiales de Madrid (ICMM-CSIC), Sor Juana Ines de la Cruz, 3, Cantoblanco, 28049 Madrid, Spain.

⁷ Unidad Asociada “Laboratorio de heteroestructuras con aplicacion en espintronica”, UCM/CSIC, Sor Juana Ines de la Cruz, 3, Cantoblanco, 28049 Madrid, Spain

E-mail: Jacobo Santamaría: jacsan@fis.ucm.es .Andres Castellanos-Gomez : andres.castellanos@csic.es

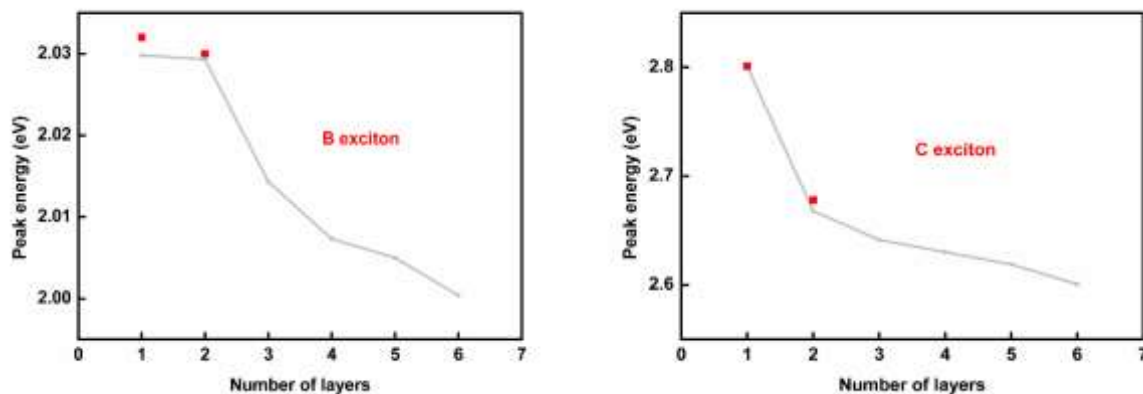


Figure S1 Thickness dependence of the B (left panel) and C (right panel) exciton peaks extracted from the spectra in Figure 2 of the main text.

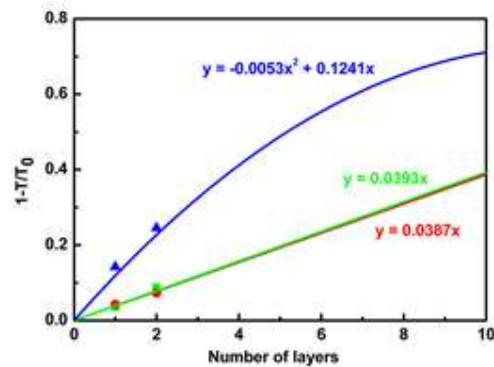


Figure S2 Thickness determination from the quantitative analysis of the transmission mode optical image of the flake on PDMS (Figure 2a of the main text). The red, green and blue lines and symbols correspond to the red, green and blue channels of the digital camera. The symbols are the experimental absorption data measured at the two locations highlighted in Figure 2a. The solid lines show the thickness expected absorption of MoS₂.

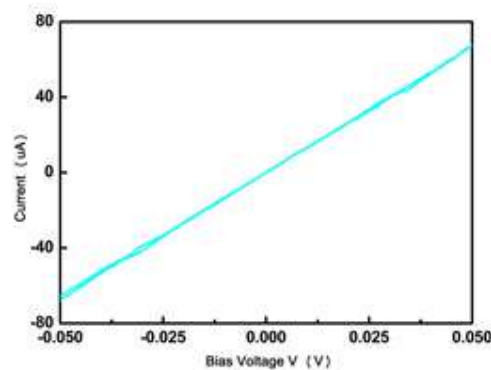


Figure S3 Current vs. bias voltage characteristics of the carbon fiber probe in contact with a gold surface to determine the resistance of the fiber probe, $R = 750 \Omega$.

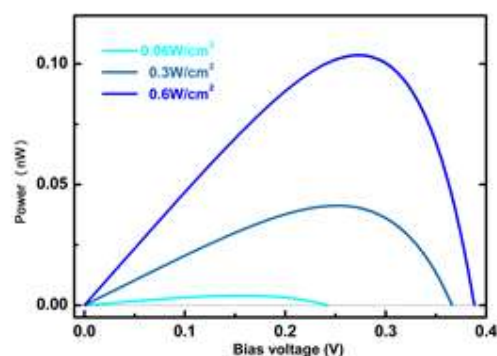


Figure S4 Photovoltaic generated power, calculated from the current vs. bias voltage characteristics shown in Figure 4b of the main text.

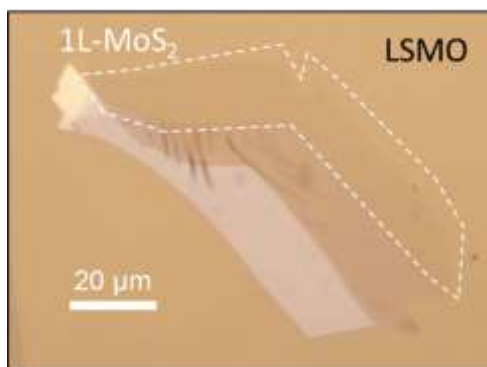


Figure S5 Epi-illumination optical image of another single-layer MoS₂ flake transferred onto a LSMO thin film.

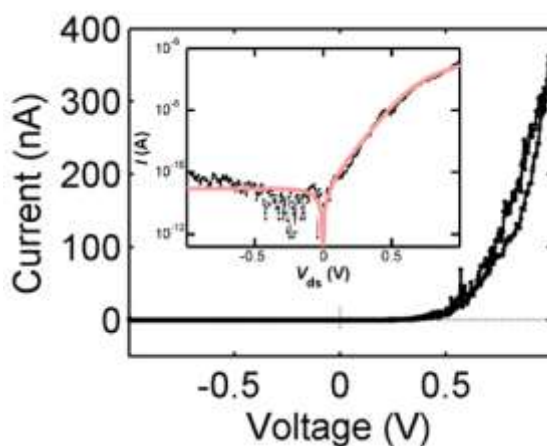


Figure S6 Current vs. bias voltage characteristics of the device shown in Figure S5. The inset shows the same dataset in semi-logarithmic scale.

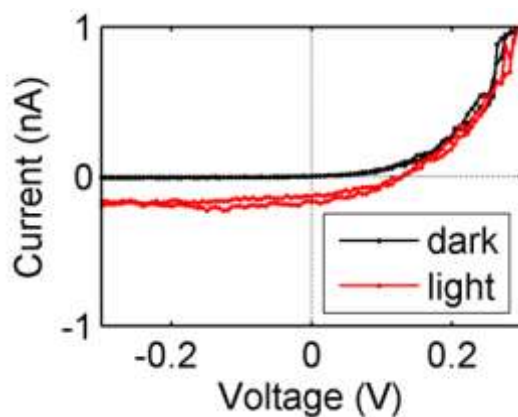


Figure S7 Current vs. bias voltage characteristics of the device shown in Figure S5 in dark and upon illumination. The characteristics upon illumination shows photovoltaic effect with $V_{oc} = 0.12$ V and $I_{sc} = 0.2$ nA. Illumination: 455 nm of wavelength and power density of 235 mW/cm².

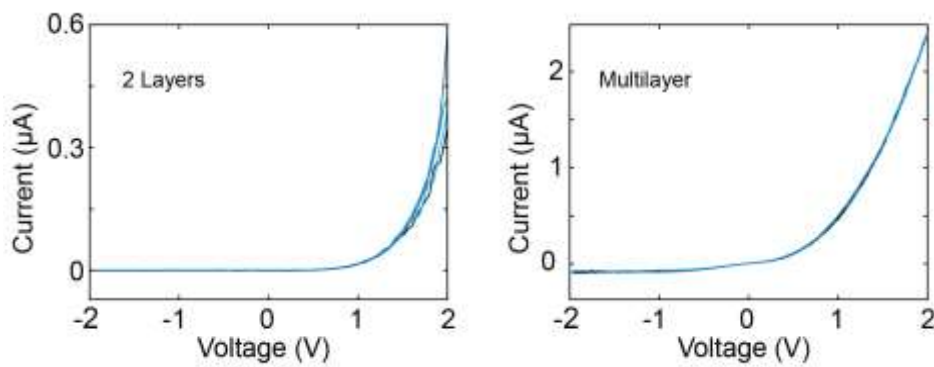


Figure S8 Current vs. bias voltage characteristics of a bilayer (left) and a multilayer (right) from device 1.

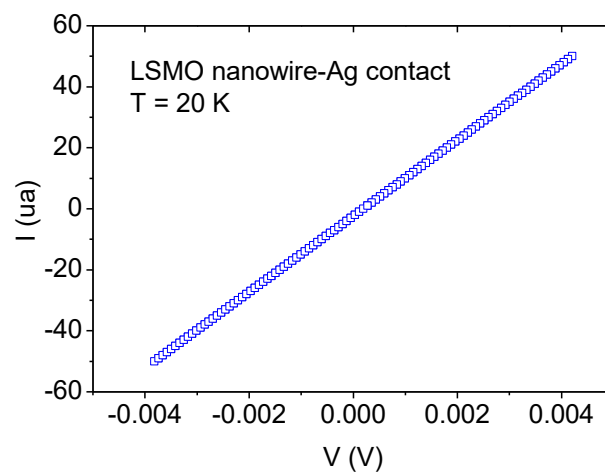


Figure S9. Current vs. bias voltage characteristics measured in a LSMO nanowire contacted with silver electrodes showing a very high current density with linear IV, indicative of Ohmic contact.